Double-Negative Mechanical Metamaterials Displaying Simultaneous Negative Stiffness and Negative Poisson's Ratio Properties

Trishan A. M. Hewage, Kim L. Alderson, Andrew Alderson, and Fabrizio Scarpa*

Dr. T. A. M. Hewage, Prof. A. Alderson
Materials and Engineering Research Institute, Faculty of Arts, Computing, Engineering and Sciences, Sheffield Hallam University, Howard Street, Sheffield, S1 1WB, United Kingdom
E-mail: A.Alderson@shu.ac.uk
Prof. K. L. Alderson
72 Phillips Lane, Formby, Liverpool, L37 4BQ, United Kingdom
Prof. F. Scarpa
Advanced Composites Centre for Innovation and Science, University of Bristol, University Walk, Bristol BS8 1TR, United Kingdom

Keywords: mechanical metamaterial, negative stiffness, negative Poisson's ratio, auxetic, mechanical properties

Intuitively, materials become both shorter and wider when compressed along their length. Here we show how a composite material or structure can display a simultaneous reversal in the direction of deformation for *both* the axial and transverse dimensions, corresponding to negative values of effective stiffness and effective Poisson's ratio, respectively. A negative Poisson's ratio[1] (NPR or auxetic[2]) host assembly stabilising (otherwise unstable) embedded negative stiffness[3] (NS) elements is presented and modelled analytically. Composite assemblies containing 3 alternative NS elements are demonstrated experimentally, confirming both NPR and NS responses under quasi-static loading over certain strain ranges and in good agreement with model predictions. We report systems demonstrating NS values over two orders of magnitude, ranging from -1.4 N mm^{-1} to -160 N mm^{-1}. Such systems are scalable and are expected to lead to increased enhancements in other useful properties such as vibration damping, finding application across transport, healthcare, defence and space sectors, amongst others.

Metamaterials derive macroscale properties from a (usually) periodic arrangement of smaller scale sub-units or building blocks. The properties are sometimes considered unknown or unusual in natural materials, and can be counter-intuitive or opposite to our everyday experience.[4,5] Metamaterials include negative refractive index[6] and negative effective mass density[7] materials finding use in, for example, electromagnetic and acoustic cloaking/lensing applications, respectively. Examples of mechanical metamaterials are negative compressibility transition,[4] NPR[1] and NS[3] materials.

Auxetic materials and structures exist, and are stable in the unconstrained state, at the nanoscale (e.g. crystalline forms of silica,[8] zeolites[9] and cellulose[10]), microscale (microporous polymers[11] and microfabricated truss-like structures[12]) and macroscale (composite laminates,[13] foams,[14,15] honeycombs[16] and patterned elastomeric spherical shells[17]). Enhanced shear modulus,[18] energy absorption[19] and indentation resistance[20] are some of the benefits known for auxetic materials and structures.[21] Periodic arrangements of sub-units leading to auxetic behaviour include truss,[16,22] corner-sharing polygon,[23,24] and hybrid truss-polygon[25] frameworks, and particle assemblies.[26,27]

NS materials and structures, on the other hand, are thermodynamically unstable unless stabilised by an external constraint.[28] Examples of NS materials include polymethacrylimide (PMI) foams,[16] honeycombs and lattices,[29,AA1,AA2] and certain crystals (VO_2, $BaTiO_3$) undergoing constrained phase transformation.[30,31] The NS effect can also be displayed by constrained buckled tube[32], buckled beam[33] or multiple magnet[34] systems. Whereas our system is demonstrated to display NS under quasi-static loading, it should be pointed out that a number of these previous studies[3,30-32] measured the dynamic modulus. Dynamic loading of NS materials can give rise to beneficial temporary effects demonstrated, for example, in

composite systems containing NS inclusions or elements which display extreme stiffness[30] and vibration damping[3,32] responses.

Our 'double-negative' mechanical metamaterial displaying simultaneous negative Poisson's ratio and negative stiffness properties comprises an auxetic host framework constraining embedded NS elements. The framework consists of a regular array of interlocked rigid hexagonal sub-units with 3 male and 3 female keys per sub-unit, arranged in an alternating fashion around the six sides of the hexagon[27] (**Figure 1**a). Assembly connectivity is via male-female key pairs formed between adjacent sub-units. When the maximum external width of the male key matches the internal width of the female key, deformation of the assembly in response to an applied mechanical load is constrained to be via cooperative translation of the rigid sub-units through relative sliding of the male and female keys along the keyways. This produces auxetic behaviour for the metamaterial. The stiffness of the metamaterial arises from each key pair containing a spring element attaching the end of the male key of one sub-unit to the base of the female key in the other sub-unit (Figure 1b).

In the Supporting Information we apply strain energy considerations to a semi-infinite array of sub-units containing multiple spring types distributed (in a regular or random manner) to predetermined keyway locations. Further, we allow spring stiffness to vary with applied global strain and to include the possibility of negative stiffness values. In this case, the effective Young's modulus in the *y* direction is:

$$E_y = \frac{3}{2}\left(\frac{4\cos^2\alpha\sum_{i=1}^{m} n_i^y k_i + \sum_{i=1}^{m} n_i^o k_i}{\cos^2\alpha}\right)\left(\frac{l_2\sin\alpha + a\cot\alpha}{l_1 + l_2\cos\alpha + a}\right) = k_y\left(\frac{l_2\sin\alpha + a\cot\alpha}{l_1 + l_2\cos\alpha + a}\right) \quad (1)$$

where l_1 and l_2 are edge lengths and α is the angle of the sub-unit (Figure 1c), a is a gap parameter (Figure 1b), m is the number of spring types, $i = 1 \ldots m$, $n_i^v = N_i^v/N$ and $n_i^o = N_i^o/N$ are the number densities of the spring having stiffness k_i in the 'vertical' and 'oblique' locations, respectively (Figure 1d), N is the total number of springs in the system, N_i^v and N_i^o are the number of springs having stiffness k_i located in vertical and oblique key positions, respectively, and k_y is the metamaterial (assembly) stiffness in the y direction.

Poisson's ratio is defined as the negative of the ratio between the strain transverse and parallel to the loading direction. The metamaterial effective Poisson's ratio expression for deformation due to cooperative sub-unit translation along the keyways is independent of spring stiffness, and obeys a reciprocal relationship:[27]

$$\nu_{yx} = \nu_{xy}^{-1} = -\frac{\left(l_2 \sin^2 \alpha + a \cos \alpha\right)}{\cos \alpha (l_1 + l_2 \cos \alpha + a)} \tag{2}$$

where ν_{yx} is the Poisson's ratio for loading in the y direction (x is the transverse direction). Note the incremental Poisson's ratio ($\nu_{yx} = -\frac{d\varepsilon_x}{d\varepsilon_y}$) has been used for Equation 2, corresponding to the negative of the slope of the transverse strain vs axial strain data in reality. The on-axis Poisson's ratios are both -1 for regular hexagonal sub-units ($l_1 = l_2$ and $\alpha = 60°$).

Consider now a buckled beam spring element. The buckled beam is a bi-stable system, generally occupying one of two c-shaped stable equilibrium states (regions (1) and (3) in **Figure 2**a) separated by an unstable snap-through transition state (region (2)). In Figure 2a the force-displacement curve has been generated using a 4th order polynomial function arbitrarily selected to generate a curve similar to the buckled beams used in the experimental

metamaterial assembly (see below). In the assembly, a buckled beam connected at its midpoint to the end of the male key by a rigid connector has its maximum negative displacement ($-\delta_{max}$) in the initial fully-expanded state. The transverse force applied to the mid-point of the buckled beam as the assembly is compressed initially meets with resistance from the buckled beam, displaying positive stiffness behaviour (region (1)). Under further compression, the stiffness of the buckled beam element changes to the extent that the beam assists rather than resists the force in displacing the system (region (2)) - it displays NS response and is stabilised under displacement control by the rigid connection to the auxetic host framework. Under high compression, the buckled beam enters region (3) where further increases in transverse beam deformation ($\delta \rightarrow +\delta_{max}$) again meet with resistance, requiring an increase in applied force (positive stiffness).

The buckled beam displacements δ_1 and δ_2 are related to the assembly geometry by $\delta_1 = \frac{\Delta_1}{3} - \frac{2a}{\tan\alpha}$ and $\delta_2 = \frac{\Delta_2}{3} - \frac{a}{\sin\alpha}$, respectively, where Δ_1 and Δ_2 are the interlock depths (maximum distance between end of male key and base of female key) in the vertical and oblique keyway locations. For rigid (infinitely stiff) sub-units, corresponding to fixed values of l_1, l_2, α, Δ_1 and Δ_2, then a is the parameter that varies under displacement control applied to the ends of the assembly (by, for example, a mechanical testing machine). In the idealised metamaterial where the width of the male interlock key matches the width of the female interlock key, the variation in a is geometrically constrained to be homogeneous throughout the assembly and applying displacement control to the end sub-units constrains internal sub-units also (i.e. they move cooperatively with the end units). The true strain of the assembly in the y direction is related to the geometry of the assembly through $\varepsilon_y = \ln\left(\frac{l_2 \sin\alpha + a\cot\alpha}{l_2 \sin\alpha + a_0 \cot\alpha}\right)$ (Equation S15 and y-directed equivalent to S10), where a_o is the value of the gap parameter in

the undeformed configuration. Hence knowledge of the assembly geometrical parameters enables the global strain to be related directly to the spring displacements. For a single buckled beam element type (Figure 2a) occupying all key positions ($m = 1$, $n_1^v = 0.333$ and $n_1^o = 0.667$) in an assembly of keyed regular hexagons, and attached at its mid-point to the end of the male key by a rigid connector in each keyway, Equation 1 predicts $k_y \propto k_1$ (Figure 2b). In this case the metamaterial displays simultaneous NPR and NS responses over the strain range where k_1 is negative.

The metamaterial stiffness can be tailored by the use of multiple spring types in the assembly. For example, replacing the buckled beams in the oblique positions with a second spring type having constant stiffness k_2 (Figure 2c and 2d; $m = 2$, $n_1^v = 0.333$, $n_1^o = 0$, $n_2^v = 0$ and $n_2^o = 0.667$) leads to an increase in strain range and magnitude of negative k_y when $k_2 < 0$. When $k_2 > 0$, the strain range and magnitude of negative k_y are diminished and disappear altogether when k_2 is sufficiently large. The minimum values of k_y and k_1 always coincide at the same strain for this configuration.

When the second spring is also a buckled beam, but having an offset force-displacement function relative to the first buckled beam (Figure 2e), achieved for example by having different length rigid connectors in the vertical and oblique keyways, then the strain range for negative k_y, and strain at minimum k_y, do not coincide with either of the buckled beam elements (Figure 2f). In Figure 2f we have used $m = 2$, $N = 54$, $N_1^v = 7$ (giving $n_1^v = 7/54 = 0.130$), $N_1^o = 26$ ($n_1^o = 0.481$), $N_2^v = 11$ ($n_2^v = 0.204$) and $N_2^o = 10$ ($n_2^o = 0.185$). This corresponds to a 3 x 3 array of unit cells with the two spring types arbitrarily distributed throughout the array to demonstrate the model is applicable to a semi-infinite assembly and is not, therefore, restricted to a single unit cell. More spring types, up to the limiting value of N

= 54 for the 3 x 3 array, are also accommodated within the semi-infinite assembly model expressions (e.g. Equation 1) but not pursued further here.

To demonstrate the double negative metamaterial concept experimentally we first establish a number of spring element configurations (**Figure 3**). A conventional spring provides a 'control' positive stiffness element (compressive axial displacement increasing with increasing compressive axial force, Figure 3a). The first example of a negative stiffness element comprises PMI foam and corresponds to axial compressive displacement in opposition to the force direction at higher compressive displacement (region (2)), following an initial positive stiffness response (region (1)) – Figure 3b. A buckled beam element displays an extended negative stiffness region (region (2)) intermediate between two stable ('c'-shaped) positive stiffness configurations (regions (1) and (3) – Figure 3c). Finally, we reproduce the buckled beam response using an assembly of 4 stationary magnets, in a square arrangement with north poles facing diagonally 'up', and a moveable magnet with north pole facing vertically 'down' (Figure 3d).

Manufactured assemblies of laser-cut interlocking regular hexagonal sub-units containing each of these element types in turn (**Figure 4**a-d) all display negative Poisson's ratios (ν_{yx}) ~ -1 (**Figure 5**a), as predicted from Equation 2. The auxetic effect is demonstrated in initial and final stills from the compression test on the magnetic assembly (Figure 4d). Supporting Information Videos S1 and S2 show the auxetic response of the magnetic and buckled beam mechanical metamaterials, respectively, undergoing compression testing. The stabilisation of the NS elements via the auxetic host framework is also clearly demonstrated in Supporting Information Video 2 for the buckled beam mechanical metamaterial. The experimental magnetic mechanical metamaterial displays homogeneous deformation via the cooperative sub-unit translation mechanism of the idealised model. On the other hand, the buckled beam

experimental mechanical metamaterial shows some buckled beam elements towards the bottom of the assembly commence the NS transition before others, accompanied by evidence of some rotation of the left-hand and right-hand side sub-units (initially at the lower portion of the assembly and then at the upper end). We attribute this to the potential for slight variation in beam and/or connecting rod lengths leading to the NS transition occuring at different global strain in different elements, and slight mis-match in male and female interlock key widths (19.65mm vs 20.25mm, respectively – **Figure S6**), allowing a small amount of sub-unit rotation for the side sub-units with free edges which is not considered in the idealised model.

The 'control' assembly containing conventional springs displays positive stiffness (k_y) for all strains investigated (Figure 5b). The assembly containing PMI foam elements, on the other hand, initially displays positive stiffness but at higher strains transitions to a double negative system displaying both negative ν_{yx} and negative k_y simultaneously. The measured control and PMI foam assembly stiffnesses agree well with the predicted values from Equation 1 using the independently measured single element stiffnesses from Figure 3a and 3b (Figure 5b), validating the analytical model and confirming the predominant deformation mode of particle translation through cooperative inter-particle sliding along keyways. Effects due to mis-match in male and female interlock key widths and/or individual spring/foam element properties of dimensions, which may lead to uneven stiffness element deformation and/or sub-unit rotation, and which would lead to a departure of the predicted response from the experimental response are, then, shown to be minor in these systems. The assemblies containing the buckled beam and magnetic (Figure 4c and 4d) spring elements both display NS at intermediate strains between initial and final positive stiffness configurations. The double negative metamaterial concept is, thus, demonstrated experimentally.

We use the validated analytical model to demonstrate we can further tune the mechanical metamaterial response by modifying the sub-unit geometry. **Figure 6**a shows the variation in incremental Poisson's ratio ν_{yx} as a function of strain ε_y for the metamaterial containing buckled beams (k_1) in the vertical locations and constant stiffness springs (k_2) in the oblique positions ($m = 2$; $n_1^v = 0.333$, $n_1^o = 0$, $n_2^v = 0$ and $n_2^o = 0.667$) for various values of sub-unit angle α (dashed curves). As α increases above the regular hexagon value of 60° the magnitude of the negative value of ν_{yx} becomes larger whilst the ε_y strain range from the fully expanded ($\varepsilon_y = 0$) to fully densified structure decreases. This is accompanied by the introduction of anisotropic mechanical response due to the reciprocal relationship between ν_{yx} and ν_{xy} (Equation 2) - the negative value of ν_{xy} becomes smaller whilst the ε_x strain range from the fully expanded ($\varepsilon_x = 0$) to fully densified structure increases as α increases above the regular hexagon value of 60° (Figure 6b).

Within the geometrical limits imposed by the fully expanded and fully densified structures, and those imposed by the sub-unit geometry, the region of ν_{yx}-ε_y space where both NPR and NS occur simultaneously is bounded by $k_y = 0$ contours in Figure 6a. For reference, points P and Q indicate the strain at which $k_y = 0$ when $\alpha = 60°$ and $k_2 = 0$ and correspond to the same points P and Q in Figure 2d. Similarly, points R and S in Figures 2d and 6a correspond to $k_y = 0$ when $\alpha = 60°$ and $k_2 = -0.25k_{10}$. For the configuration considered in Figure 6, the double negative metamaterial exists over a larger range of ν_{yx}-ε_y space as k_2 decreases. The mechanical response of this metamaterial can be further tuned by varying sub-unit edge lengths (**Figure S1** and **S2**), and employing alternative/additional spring types (**Figure S3**).

Figures 6a,b and S1-S2 show it is possible to design the mechanical metamaterial with extreme values of the mechanical properties by employing sub-unit geometrical parameters

leading to high aspect ratio sub-units. So, for example, if a large magnitude negative value of incremental Poisson's ratio is required then Figure 6a demonstrates this will be achieved for ν_{yx} when $\alpha \rightarrow 90°$. This corresponds to a high aspect ratio sub-unit with the long axis aligned along the y direction. Note, however, that whilst the length of the sub-units and, therefore, assembly increase in the loading direction as $\alpha \rightarrow 90°$ (or l_2 increases) the maximum displacement due to sub-unit translation along the keyways remains the same, leading to the decrease in loading ε_y strain range noted above. Similar arguments apply to ν_{xy} and ε_x range when α tends to low values (22.5° for the system in Figure 6b) or l_1 increases (Figure S1). If an increase in both the magnitude of the incremental negative Poisson's ratio and the loading strain is desired, Figure S2 shows this is achieved for ν_{xy} and ε_x by decreasing l_2 towards its minimum value. This achieves high sub-unit aspect ratio and also a reduction in assembly length along the loading direction to provide increases in both the magnitude of Poisson's ratio and loading strain range, respectively. The stiffness of the system (k_y and k_x) in each direction is determined by the spring element force constants and the sub-unit angle (e.g. Equation 1 and equivalent term on right hand side of Equation S17). Trivially, the more negative the spring constants of the elements the more negative the stiffness of the overall assembly. Extreme particle aspect ratios yield extreme stiffness values and large negative k_y and k_x are achieved as $\alpha \rightarrow 90$ and 0°, respectively. The metamaterial Young's moduli have an additional dependence on sub-unit lengths (Equations 1 and S17) – large negative E_y is achieved as l_1 decreases and l_2 decreases, with E_x showing the reverse dependency on these parameters.

Returning to the force-displacement response of the buckled beam system (Figure 5b), steps are evident at ~5 and 10 mm displacement and these are attributed to the sequential or staggered on-set of the NS buckling response in individual beam elements noted above.

Sequential buckling of rows of buckled beams[29,AA1,36] and other hinged/buckled systems[AA2] is known to occur due to the strongly non-linear response of such multistable metamaterials. Indeed, sequential buckling, caused by small imperfections in the elements, has been deliberately designed into lattices for enhanced energy absorption.[29,AA1,36] The effective stiffness k of such systems follows a series arrangement of row stiffnesses k_i^{row}, i.e. $k = \left(\sum_{i=1}^{m} N_i / k_i^{row} \right)^{-1}$, where here m is the total number of rows, and N_i is the number of rows having row stiffness k_i^{row}. The deformation of such systems is inhomogeneous throughout the lattice – occurring row-by-row, rather than all rows at the same time, and occurs in order of the collapse stress of each row.

For the mechanical metamaterial presented in this work comprising of a semi-infinite assembly of interlocking hexagonal sub-units, when the width of the male interlock key matches the width of the female interlock key then cooperative translation of the sub-units along the sub-unit keyways occurs. A distinctive feature then of the concept presented here is that the deformation is homogeneous throughout the assembly and it is not possible in the idealised assembly for one sub-unit, row of sub-units, or localised group of sub-units to move (or collapse) without all other sub-units moving in the same manner. This is consistent with the absence of any stiffness element term in the Poisson's ratio expression (Equation 2), and leads to an effective stiffness according to a parallel (rather than series) arrangement of elements (i.e. the weighted average expression in Equation 1). In the case of interlocking regular hexagonal sub-units, this precludes sequential on-set of the NS transition in identical elements located in different keyways of the assembly.

In reality, a degree of tolerance may be required between the male and female key widths and, therefore, some contribution from rotation of the sub-units to the deformation of the

mechanical metamaterial. This would allow some sequential on-set of NS transitions to take place in distributed identical elements. The semi-infinite assembly model does not account for sub-unit rotation but can, nevertheless, be applied for the prediction of the effects of sequential buckling (due to sub-unit rotation) on the overall stiffness response of the system. For example, **Figure 7**a shows three arbitrarily off-set buckled beam curves. The curves for spring types 2 and 3 each show a correspondingly slightly larger amplitude and period than spring type 1 to account for inherent variability due to manufacturing in a real system – shown to better effect in Figure 7b where the curves are presented without off-set. The response of a 3 x 3 array of unit cells with spring type 1 occupying all keyways ($m = 1$, $N = 54$, $n_1^v = 0.333$, $n_1^o = 0.667$) is compared to that of a 3 x 3 array containing equal numbers of off-set springs 1, 2 and 3 distributed evenly throughout the system ($m = 3$, $N = 54$, $n_1^v = n_2^v = n_3^v = 0.111$, $n_1^o = n_2^o = n_3^o = 0.222$) in Figure 7c (solid and dashed curves, respectively). The presence of off-set buckled beams modifies the effective stiffness response significantly, including the presence of steps consistent with those in the force-displacement response of the experimental buckled beam system (Figure 5b).

The sub-unit rotation mechanism giving rise to the staggered on-set of the NS response will be particularly evident for sub-units at the edges of the assembly due to the incomplete set of neighbours for these sub-units. The small finite assemblies tested experimentally (Figure 4) then represent a worst case scenario in this respect and we expect the steps in the force-displacement response for the buckled beam system would be less evident as the contribution due to sub-unit rotation diminishes with increasing number of sub-units in the assembly. However, increasing the number of sub-units and potentially, therefore, number of elements increases the likelihood of sequential NS transition on-set due to imperfections in the elements themselves. Note, however, that this is confined to individual elements, rather than whole rows in the previously reported sequential buckling systems. The model predictions for

the 3D array with spring types 1-3 without off-set (representing variabilty due to imperfections – Figure 7b) are shown by the dot-dashed curve in Figure 7c. The predictions indicate the modification to the response from that of the array with uniform distribution of spring type 1 only will be less than that for the off-set spring types (i.e. when sub-unit rotation is significant). For the level of variability employed in spring types 1-3, the ‘parallel‘ nature of the effective stiffness response in Equation 1, as a consequence of the homogeneous deformation of the interlocking assembly, means that steps are not present in the effective stiffness response. This is contrary to the previously reported honeycomb systems, or the current mechanical metamaterial when sub-unit rotation is significant.

The double negative metamaterial concept presented here needs not be restricted to either the auxetic host framework or negative stiffness guest elements considered above. In addition to particle assemblies, negative stiffness elements can be envisaged to be constrained within 2D truss,[16,22] connected polygon[23] and truss-polygon[25] frameworks, and their 3D counterparts.[12,24] The effects are also independent of scale, with microfabrication techniques enabling scaling down to micron-sized features,[5,12] whilst molecular analogues (e.g. to the interlocking hexagon framework and buckled beams in the form of ‘hard cyclic multimer’ assemblies[26] and buckled nanotubes,[35] respectively) provide intriguing possibilities. Naturally, there will be issues of robustness, efficiency, reliability and, in the case of the magnetic system, potential for interference between magnets associated with different sub-units when scaling down the assembly. Nevertheless, in this respect, the recent successful microfabrication using 3D laser lithography of 3D polymer microlattice structures incorporating buckled beam elements, all using a single material, is especially noteworthy.[36] Microlattices displaying repeatable yet irreversible energy absorption, and also self-recovery, were reported. No damage was observed following 80 load-unloading cycles, and overall hysteresis behaviour remained largely unchanged, demonstrating a degree of robustness and

reliability. Clearly this could be extended to auxetic microlattices containing built-in buckled beam elements as per the concept demonstrated here. Buckled beams have also been incorporated as elements connecting resonating metal masses to surrounding elastomeric matrix to produce a tunable and switchable acoustic metamaterial.[37] Considering non near-neighbouring magnetic interactions, at the nanoscale these interactions tend to be significantly reduced because the magnetic forces scale with r^6.[38] From a materials perspective, at the nanoscale the influence of non near-neighbouring effects may simplify the magnetic design significantly.

A recent review of approaches and challenges for achieving negative elastic moduli provides alternative options for NS constituents under dynamic loading.[39] This includes a simple-cubic lattice of metal-rubber core-shell spheres embedded within a host material, where negative effective values of the mass density and/or of the elastic moduli can be achieved by appropriate selection of the resonance frequencies of the core-shell unit and the lattice.[40] An oscillating system of masses and springs shows resonances with three independent negative elastic moduli and negative scalar mass density.[41] A single-phase material chiral microstructure has been developed which possesses simultaneous negative effective mass density, bulk modulus and refraction of elastic waves at the deep-subwavelength scale due to simultaneous translational and rotational resonances in hexagonal sub-units.[42] A novel extension of the interlocking hexagon system reported here might include architecturing the hexagonal sub-units in our assembly with the chiral microstructure to give multiple resonances for improved multifunctionality.

The magnetic NS mechanism allows electromagnetic active control, in addition to mechanical displacement control, to switch on or off the NS effect. Embedded magnets have been employed to enable elastomeric kagome lattice structures to display magneto-elastic

reconfigurable properties, switching between open and closed equilibrium states, but neither negative Poisson's ratio nor negative stiffness were claimed in these systems.[43] Stabilisation of the NS property can be achieved by sandwiching the metamaterial between stiff outer skins or, for scaled down double negative metamaterial inclusions, embedding within a matrix (similar to the previous reports on NS inclusion composites[3,30,32]). Forseeable benefits of the "double negative" response described here include a sandwich panel with aligned skin and core planes which would present excellent drape (due to the tendency for synclastic curvature under bending of an auxetic core)[14,44] and damping (in-plane auxetic and NS core),[3,19,32] combined with high in-plane stiffness (skin) and through-thickness stiffness (core) for structural aspects. The high volume change of the auxetic host also provides the potential for a damping structure (due to the NS elements) that is deployable from a small volume configuration for transportation to a large volume in the final deployed state. The high volume change in auxetic porous materials has also been shown to lead to tuneable response mass filters[45], and the wave propagation in cellular lattice phononic filters is known to be dependent on topology and stiffness with different responses for auxetic and non-auxetic systems.[46] The presence of mechanically- or magnetically-activated snap-through NS elements provides an enhanced mechanism for providing dramatic porosity (and cell shape) variation to provide instantaneous and complete opening of the auxetic filter pores for cleaning of foulant from a mass filter or to alter the band gap in a phononic material, for example. Consequently, applications for such double negative metamaterials are likely in, but not limited to, aerospace components, vibration damping tables, neonatal transporters, impact protectors, sensors and actuators, smart deployable and morphing structures, and MEMs devices.

Experimental Section

Fabrication of Spring Elements: Conventional positive stiffness springs, 5 mm in diameter and 12 mm in length, were supplied by RS Components Ltd. PMI foam (200WF, 205 kg m^{-3}, supplied by Rohacell) samples of dimensions 25 mm × 25 mm × 35 mm were cut from a larger block for compression testing along the foam rise direction. Smaller PMI foam samples (5 mm (rise direction) × 10 mm × 10 mm) were cut for incorporation into the interlocked hexagon assembly. Buckled beams were created by cutting a general purpose steel tape measure into 35 mm x 5 mm x 0.5 mm steel strips. A hole was created at the midpoint of each strip and attached to the free end of a square cross-section copper tube (the rigid connector) via a nail and glue (inside the copper tube). A single strip was located in slits in opposing internal walls of a U-shaped holder (acrylic) having an internal width of (28 mm) to create the buckled beam specimen for compression testing (**Figure S4**). The 5-magnet system concept demonstrator (Figure 3d) was created using corrugated board in which a series of square holes were created, using a laser cutter, along directions at ± 45 ° to the horizontal direction to accommodate the 4 stationary neodymium block magnets (part number C0350, supplied by SuperMagnetMan). The mobile block magnet was placed inside a holder for attachment to the mechanical testing machine along the vertical bisector of the magnetic quadrupole formed by the 4 stationary magnets. The magnets used in the interlocked hexagon assembly were neodymium bar magnets (NdFeB, grade N42, part number B422, supplied by KJ Magnetics) with dimensions of 6.35 mm × 3.175 mm × 3.175 mm.

Fabrication of Interlocked Hexagon Assemblies: A CAD model of the sub-unit for each assembly was exported to a laser cutting machine (World Lasers LR1612 laser cutter (40 W CO_2 laser) for the PMI assembly; Trotec Speedy 400 laser cutter (80 W CO_2 laser) for the control, buckled beam and magnet assemblies). For the PMI assembly a 12 mm thick transparent perspex sheet was used as the base material from which individual sub-units (**Figure S5**) were cut. The sub-units were subsequently polished and greased to minimise the

friction between the male and female keys. The assembly comprised of seven sub-units (Figure 4b). White acrylic paint was applied to the surface of the initially transparent sub-units and black dots were marked at equivalent points on the terminals of the male keys to provide fiducial markers for subsequent strain determination. Two PMI foam elements were placed in the central vertical keyway positions of the assembly and attached to the adjacent sub-units using double-sided adhesive tape. Lower modulus open-cell polyurethane foam inserts were placed in other keyways to minimise rotation of sub-units due to edge effects, and movement of sub-units due to their own weight, and thus ensure translation of sub-units along the keyways was the predominant deformation mode in response to compressive loading of the assembly. To avoid out-of-plane buckling during compression testing, the assembly was sandwiched between two 4 mm thick transparent perspex face sheets connected to each other by four copper wire bands. A 12 mm × 10 mm × 4 mm perspex cuboid, glued to the middle of the painted surface of each sub-unit, minimised friction between the painted surface and the face plate.

The sub-units for the buckled beam assembly were constructed from three separate 3 mm thick layers (Figure S6). The bottom and middle layers were cut from opaque yellow acrylic sheet whereas the top layer was a transparent acrylic. The middle layer included the male and female keys, with a slit at the end of each male key to accommodate the rigid connection to the associated buckled beam element, and slits on either side of the opposing internal female key walls to house the buckled beam itself. The width of the male key was slightly smaller than the female key width to assist sub-unit translation by reducing friction between the key surfaces. The top and bottom layers were cut to the shape of a regular hexagon having edge length equal to the edge length of the keyed middle layer. Each layer of the sub-unit contained four locating holes to ensure layer alignment when constructing the sub-unit. A steel strip (as described above) was attached at its mid-point to the rigid connector of the male key, and the

ends of the steel strip were inserted into the slits either side of the female key. The steel strip became naturally buckled due to having a longer length than the width of the female key. Since the degree of buckling is determined at this stage by the length of the strip and the width of the female key, there is no directional dependency on the ease of buckling during fabrication. Of course, during subsequent mechanical testing the ease of buckling for any given element is determined by the location of the element within the assembly and its orientation with respect to the direction of loading (being easier to buckle when located in a keyway aligned along the loading direction). This is accounted for in the strain energy approach to deriving the model expressions for the mechanical metamaterial effective Young's moduli (Equations S1 to S18) and the subsequent comparison of the model with experiment (Equations S19 to S26). Buckled beams were distributed in this manner throughout the assembly of middle layer sub-unit sections and grease was applied on the male keys to reduce friction. The top and bottom hexagon layers were then attached to the middle layer of each sub-unit using 3 mm screw nails in the 4 locating holes of each layer. Washers were placed between each layer to minimise friction in the key ways. The top and bottom layers of the sub-units prevent the system from buckling out of plane and so face sheets were not required for the buckled beam assembly during subsequent testing (Figure 4c).

A 3-layer grooved sub-unit, and similar layer construction procedure, was also used for the Magnets assembly. Sub-unit layers where cut from white Perspex sheet. The mobile magnet was placed in a rectangular hole located at the terminal of the male key in the top layer, while the 4 stationary magnets were arranged in rectangular holes around the top layer female key (**Figure S7**). Tape was applied to hold the magnets securely in the accommodating holes of the top layer.

Fabrication of the 'Control' assembly was similar to that of the buckled beam assembly, with the buckled beam elements replaced by the positive stiffness springs. A layered sub-unit was assembled following a similar scheme to the buckled beam assembly sub-unit (all 3 layers cut from yellow acrylic, **Figure S8**).

Mechanical Testing: The individual PMI foam compression test specimens were sandwiched between two polypropylene sheets and subjected to compression testing in an Instron 3369 mechanical testing machine fitted with a 25 kN load cell at a displacement rate of 5 mm min^{-1}. The single buckled beam sample (Figure 3c and Figure S4) and single conventional spring samples (Figure 3a) were both compression tested in an Instron 3369 (50 kN load cell, 10 mm min^{-1} displacement rate). The 5-magnet system concept demonstrator (Figure 3d) was compression tested in an Instron 3369 (25 kN load cell, 10 mm min^{-1} displacement rate).

Mechanical characterisation of the PMI foam assembly was carried out using a MESSPHYSIK ME46-NG video extensometer, employing a tripod-mounted Digitale CMOS Kamera ueyele 752 x 480 1/3'' camera with high precision zoom lens (TAMRON 1110522 JAPAN, 1: 1.6, 25 mm). The video extensometer dot matrix x-y strain mapping capability allowed measurement of local strains of the test specimen undergoing compression testing in an Instron 3369 mechanical testing machine fitted with a 50 kN load cell. Tests were performed at a displacement rate of 2 mm min^{-1}. Field-of-view x and y coordinates for each fiducial dot marker were recorded throughout the duration of the compression test, with y corresponding to the axial (loading) direction and x the transverse direction. Dot pairs (A,B), (C,D) and (E,F) (Figure 4b), corresponding to two repeat unit-cell lengths along the y direction, were used to determine the axial true strain (ε_y). Dot pairs (G,H), (I,J) and (K,L), separated by one repeat unit-cell length along the x direction, were used to determine the transverse true strain (ε_x). For example, the local axial true strain was determined from point

pair (A,B) using $\varepsilon_y = \ln \frac{\left(y_B^d - y_A^d\right)}{\left(y_B^0 - y_A^0\right)}$ where y_A and y_B are the y coordinates for points A and B, and the superscripts 0 and d correspond to initial and instantaneous (deformed) values, respectively. The global true loading strain was determined using $\varepsilon_y = \ln\left(\frac{Y}{Y_0}\right)$ with the instantaneous (Y) and initial (Y_0) lengths in the y direction given by the separation of the jaws during and at the start of the test, respectively.

The buckled beam, magnet and control assemblies were compression tested in an Instron 3369 (50 kN load cell, 10 mm min^{-1} displacement rate), and digital photographs taken every 5 seconds from the beginning of the test using a high resolution digital camera (CANON 5D Mark II) with 24-105 mm high precision zoom lens and image stabilizer attached. The digital images were subsequently imported in to the "ImageJ" image processing software to generate the coordinates of the screw heads (Figure 4a, 4c and 4d) on each sub-unit. Local and global strains were then generated using the same protocol as for the PMI foam assembly. Force-displacement data were generated directly by the Instron testing machine for all single element (Figure 3) and assembly (Figure 5b) tests.

Acknowledgements
The study arose from preliminary work in collaboration with Dr M. R. Haberman of The University of Texas at Austin, USA. TAMH was supported by funding from the US Army Research Office, Sheffield Hallam University and the University of Bolton, and is grateful to Prof C. Sammon of Sheffield Hallam University for PhD co-supervision. TAMH undertook design, fabrication and testing of whole assemblies and assembly constituents, the development and use of the analytical model expressions, and data analysis as part of his PhD project under the supervision of KLA and AA. FS was responsible for identifying and guiding the use of foams as NS elements within the double negative mechanical metamaterial, and provided additional guidance on NS stabilisation as an Advisor to TAMH's PhD project. KLA devised the programme of novel mechanical inclusions for vibration damping and related applications, and oversaw aspects of mechanical testing and analysis. AA developed the concept of incorporating NS elements within an NPR host framework, contributed to the development and use of the analytical model expressions, and contributed to the mechanical testing and analysis. All authors contributed to the preparation of the manuscript, which was led by AA.

[1] G. N. Greaves, A. L. Greer, R. S. Lakes, T. Rouxel, *Nature Mater.* **2011**, *10*, 823.

[2] K. E. Evans, M. A. Nkansah, I. J. Hutchinson, S. C. Rogers, *Nature* **1991**, *353*, 124.

[3] R. S. Lakes, T. Lee, A. Bersie, Y. C. Wang, *Nature* **2001**, *410*, 565.

[4] Z. G. Nicolaou, A. E. Motter, *Nature Mater.* **2012**, *11*, 608.

[5] M. Kadic, T. Bückmann, R. Schittny, M. Wegener, *Rep. Prog. Phys.* **2013**, *76*, 126501 (34pp).

[6] R. A. Shelby, D. Smith, S. Schultz, *Science* **2001**, *292*, 77.

[7] S. Zhang, L. Yin, N. Fang, *Phys. Rev. Lett.* **2009**, *102*, 194301.

[8] Y. Yeganeh-Haeri, D. J. Weidner, J. B. Parise, *Science* **1992**, *257*, 650.

[9] J. N. Grima, R. Jackson, A. Alderson, K. E. Evans, *Adv. Mater.* **2000**, *12(24)*, 1912.

[10] K. Nakamura, M. Wada, S. Kuga, T. Okano, *J. Polym. Sci. Part B: Polym. Phys.* **2004**, *42(7)*, 1206.

[11] B. D. Caddock, K. E. Evans, *J. Phys. D: Appl. Phys.* **1989**, *22*, 1877.

[12] T. Bückmann, N. Stenger, M. Kadic, J. Kaschke, A. Frölich, T. Kennerknecht, C. Eberl, M. Thiel, M. Wegener, *Adv. Mater.* **2012**, *24*, 2710.

[13] C. Herakovich, *J. Comp. Mat.* **1984**, *18*, 447.

[14] R. Lakes, *Science* **1987**, *235*, 1038.

[15] Y. Li, C. Zeng, *Adv. Mater.* **2016**, *28*, 2822.

[16] L. J. Gibson, M. F. Ashby, *Cellular Solids: Structure and Properties*, Pergamon Press, London, **1988**.

[17] S. Babaee, J. Shim, J. C. Weaver, E. R. Chen, N. Patel, K. Bertoldi, *Adv. Mater.* **2013**, *25*, 5044.

[18] J. B. Choi, R. S. Lakes, *J. Mater. Sci.* **1992**, *27*, 5375.

[19] B. Howell, P. Pendergast, L. Hansen, *Acoustic behaviour of negative Poisson's ratio materials*, DTRC-SME-91/01, David Taylor Research Centre Annapolis MA, **1991**.

[20] K. L. Alderson, A. P. Pickles, P. J. Neale, K. E. Evans, *Acta Metall. Mater.* **1994**, *42*, 2261.

[21] K. E. Evans, A. Alderson, *Adv. Mater.* **2000**, *12*, 617.

[22] U. D. Larsen, O. Sigmund, S. Bouwstra, *J. Microelectromechanical Systems* **1997**, *6*, 99.

[23] J. N. Grima, K. E. Evans, *J. Mater. Sci. Lett.* **2000**, *19*, 1563.

[24] A. Alderson, K. E. Evans, *Phys. Rev. Lett.* **2002**, *89(22)*, 225503-1.

[25] K. E. Evans, *J. Phys. D: Appl. Phys.* **1989**, *22*, 1870.

[26] K. W. Wojciechowski, *Molecular Physics* **1987**, *61*, 1247.

[27] N. Ravirala, A. Alderson, K. L. Alderson, *J. Mater. Sci.* **2007**, *42*, 7433.

[28] R. S. Lakes, W. J. Drugan, *J. Mech. Phys. Solids* **2002**, *50*, 979.

[29] D. M. Correa, C. C. Seepersad, M. R. Haberman, *Integrating Materials and Manufacturing Innovation* **2015**, *4:10*.

[AA1] D. Restrepo, N. D. Mankame, P. D. Zavattieri, *Extreme Mechanics Letters* **2015**, *4* 52.

[AA2] B. Haghpanah, L. Salari-Sharif, P. Pourrajab, J. Hopkins, L. Valdevit, *Adv. Mater.* **2016**, in press.

[30] Y. C. Wang, M. Ludwigson, R. S. Lakes, *Mater. Sci. Eng. A* **2004**, *370*, 41.

[31] T. Jaglinski, D. Kochmann, D. Stone, R. S. Lakes, *Science* **2007**, *315*, 620.

[32] R. S. Lakes, *Phil. Mag. Lett.* **2001**, *81(2)*, 95.

[33] C. Coulais, J. T. B. Overvelde, L. A. Lubbers, K. Bertoldi, M. van Hecke, *Phys. Rev. Lett.* **2015**, *115*, 044301.

[34] R. Ravaud, G. Lemarquand, V. Lemarquand, *IEEE Transactions on Magnetics* **2009**, *45(9)*, 3334.

[36] T. Frenzel, C. Findeisen, M. Kadic, P. Gumbsch, M. Wegener, *Adv. Mater.* **2016**, *28*, 5865.

[35] H. W. Yap, R. S. Lakes, R. W. Carpick, *Phys. Rev. B* **2008**, *77*, 045423.

[37] P. Wang, F. Casadei, S. Shan, J. C. Weaver, K. Bertoldi, *Phys. Rev. Lett.* **2014**, *113,* 014301.

[38] A. Akbarzadeh, M. Samiei, S. Davaran, *Nanoscale Research Letters* **2012**, *7*, 144.

[39] J. Christensen, M. Kadic, M. Wegener, O. Kraft, *MRS Communications* **2015**, *5*, 453.

[40] Z. Liu, X. Zhang, Y. Mao, Y.Y. Zhu, Z. Yang, C.T. Chan, P. Sheng, *Science* **2000**, *289*, 1734.

[41] Y. Lai, Y. Wu, P. Sheng, Z.-Q. Zhang, *Nat. Mater.* **2011**, *10*, 620.

[42] R. Zhu, X.N. Liu, G.K. Hu, C.T. Sun, G.L. Huang, *Nat. Commun.* **2014**, *5*, 5510.

[43] M. Schaeffer, M. Ruzzene, *J. Appl. Phys.* **2015**, *117*, 194903.

[44] K. E. Evans, *Compos. Struct.* **1991**, *17*, 95.

[45] A. Alderson, J. Rasburn, S. Ameer-Beg, P. G. Mullarkey, W. Perrie, K. E. Evans, *Ind. Eng. Chem. Res.* **2000**, *39*, 654.

[46] M. Ruzzene, F. Scarpa, Phys. Stat. Sol. B **2005**, *242*, 665.

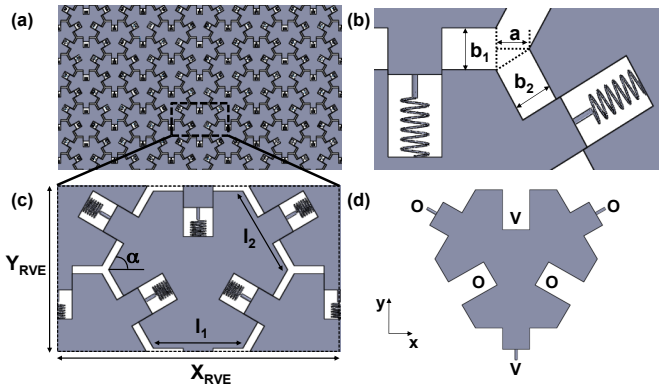

Figure 1. Mechanical metamaterial design of auxetic framework with constrained embedded spring elements. a) Extended interlocking hexagon assembly with spring elements located in the key-keyway interlocks. Each hexagon sub-unit has two edges of length l_1 along the x direction, and four edges of length l_2 oriented at an angle of α to the x direction. b) Expanded view of a key-keyway interlock. c) Representative volume element. d) Individual hexagonal sub-unit showing vertical and oblique positions of the keys/keyways.

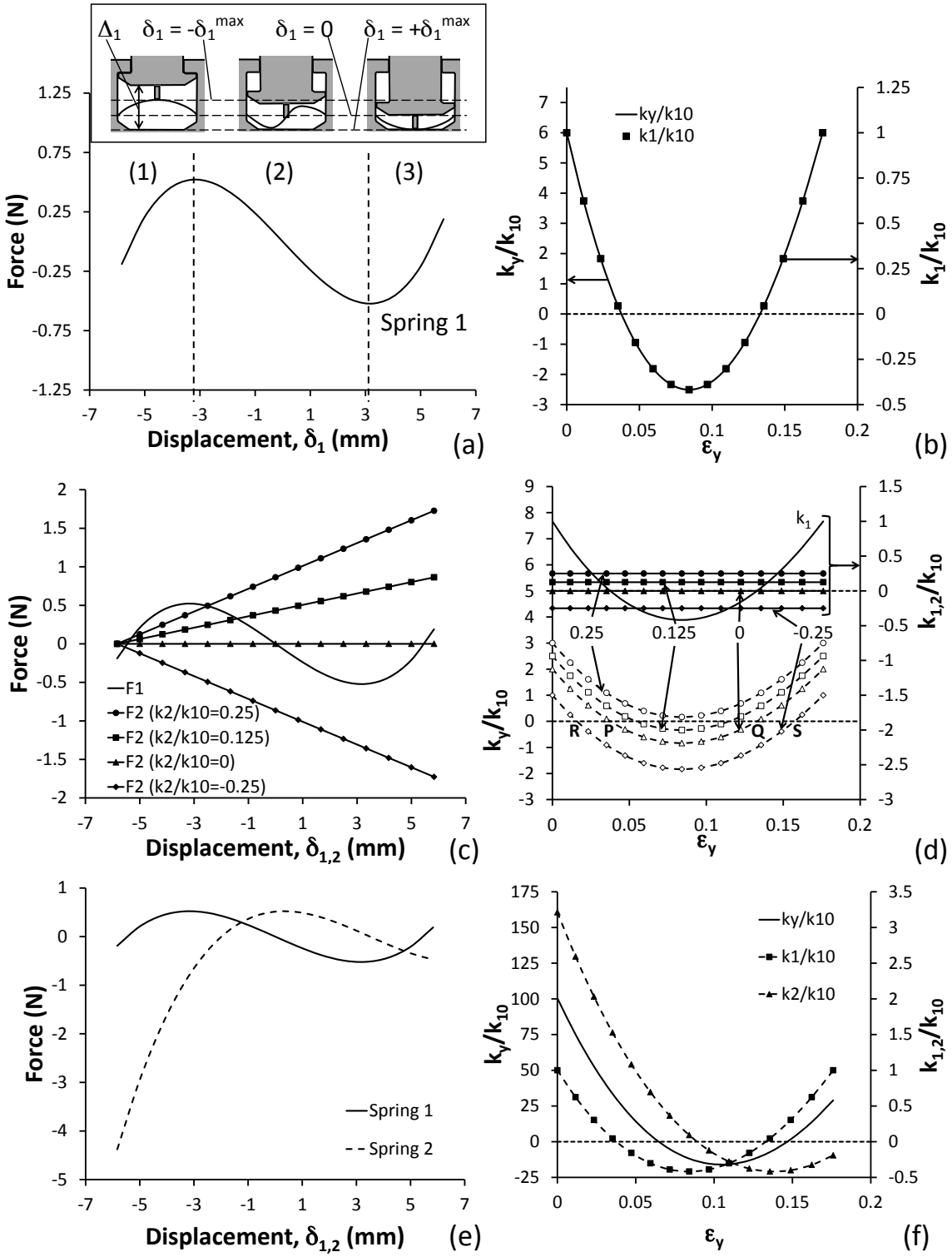

Figure 2. Predicted metamaterial stiffness responses for different spring configurations in an assembly of keyed regular hexagons. $l_1 = l_2 = 35$ mm, $\alpha = 60°$, $\Delta_1 = \Delta_2 = 0.5l_1$, $a_0 = 0.288l_1$, $\delta_{10} = \delta_{20} = \delta_0 = -0.167l_1$. a) Typical force-displacement curve for a buckled beam ($F = [-(\delta/l_1)^4 + 4{,}230.8(\delta/l_1)^3 + 0.01563(\delta/l_1)^2 - 103.91(\delta/l_1) + 0.0001]/12$). b) Metamaterial stiffness (k_y) and spring stiffness (k_1 - derived from slope of force-displacement curve in (a), normalised to the zero strain spring stiffness (k_{10}), as a function of global applied compressive strain (ε_y) for a single buckled beam spring type occupying all key locations ($n_1^v = 0.333$ and $n_1^o = 0.667$).

c) Typical force-displacement curves for a buckled beam (as in (a)) and springs having constant stiffness k_2 equal to $-0.25k_{10}$, 0, $0.125k_{10}$ and $0.25k_{10}$. d) Normalised metamaterial stiffness (k_y/k_{10} - dashed lines, empty symbols) and spring stiffness (k_i/k_{10} - solid lines, filled symbols) as a function of ε_y for a buckled beam spring type (k_1 derived from (a), (c)) occupying all vertical key locations ($n_1^v = 0.333$ and $n_1^o = 0$) and a constant stiffness spring type ($k_2 = -0.25k_{10}$, 0, $0.125k_{10}$ and $0.25k_{10}$) occupying all oblique key locations ($n_2^v = 0$ and $n_2^o = 0.667$). Points P and Q correspond to the strains where $k_y = 0$ when $k_2 = 0$, and points R and S to the strains where $k_y = 0$ when $k_2 = -0.25k_{10}$. e) Force-displacement curves for two offset buckled beams (spring 1 as in (a), (c), spring 2: $F = [-(\delta/l_1)^4 + 4{,}231.2(\delta/l_1)^3 - 1269.3(\delta/l_1)^2 + 23.015(\delta/l_1) + 6.1604]/12$). f) Normalised metamaterial stiffness (k_y/k_{10}) and spring stiffness (k_i/k_{10}) as a function of ε_y for a buckled beam spring type (k_1 derived from (a), (c)) and a second (offset) buckled beam spring type (k_2 derived from slope of spring 2 function in (e)) arbitrarily distributed in a 3 x 3 unit cells assembly with $n_1^v = 0.130$ and $n_1^o = 0.481$, $n_2^v = 0.204$ and $n_2^o = 0.185$.

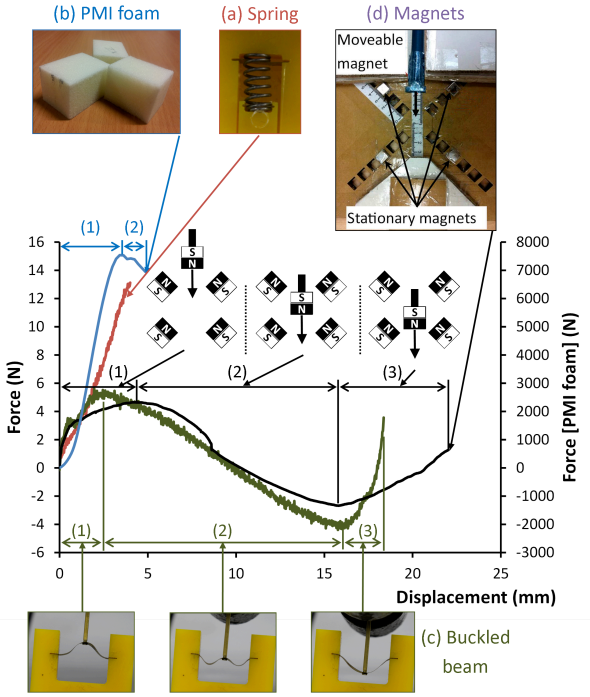

Figure 3. Spring element configurations. a) Conventional (control) spring showing monotonically increasing compressive force-displacement behaviour characteristic of positive stiffness response. b) PMI foam displaying positive stiffness response in region (1) followed by negative stiffness (decreasing compressive force for increasing compressive displacement) in region (2). c) Buckled beam displaying positive stiffness responses at low and high compressive strain (regions (1) and (3)) and negative stiffness response at intermediate strain (region (2)). d) 5-magnet assembly displaying similar response to buckled beam: positive stiffness in region (1) occurs due to repulsion between the north pole of the moveable magnet and the north poles of the top two stationary magnets providing resistance to the compressive force vertically; in region (2) the repulsion between the north poles of the moveable magnet and the top two stationary magnets assists the force in displacing the system (i.e. reversal of the direction of deformation with respect to the force) corresponding to negative stiffness; repulsion between the north poles of the moveable magnet and the bottom two stationary magnets returns the system to positive stiffness response in region (3).

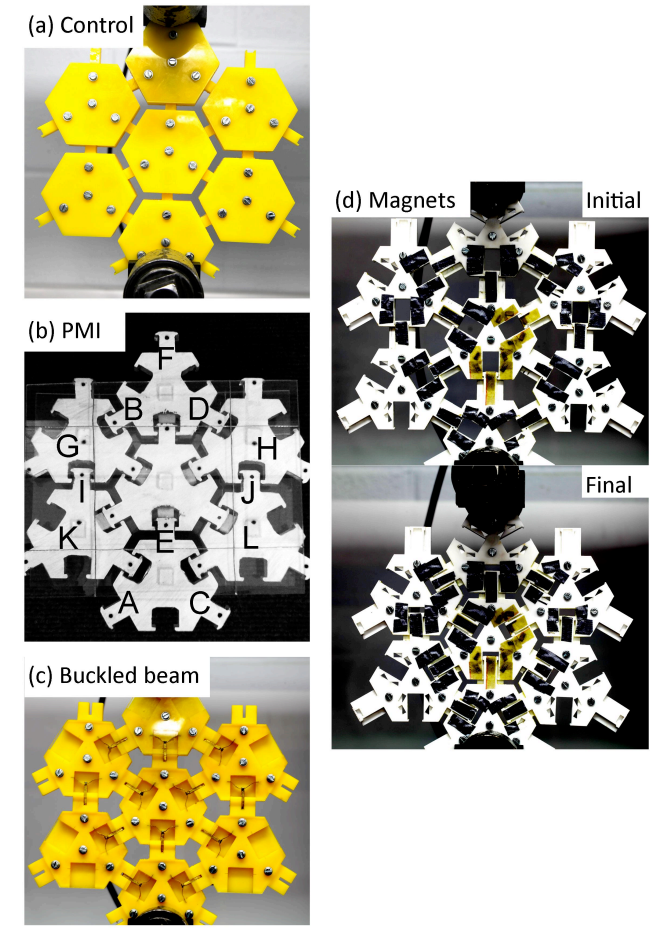

Figure 4. Interlocking hexagon assemblies and corresponding transverse contractile strain vs compressive axial strain data and compressive force vs displacement data. a) Assembly containing single conventional spring type occupying all key locations, corresponding to n_1^v = 0.333 and n_1^o = 0.667. b) Assembly containing two PMI foam elements in the central vertical keyway positions (n_1^v = 0.167 and n_1^o = 0) and lower modulus open-cell polyurethane foam inserts in other keyways (n_2^v = 0.167 and n_2^o = 0.667) to minimise rotation of units due to edge effects, and thus ensure translation of units along the keyways was the predominant deformation mode in response to compressive loading of the assembly. Two 4mm thick transparent perspex face sheets connected to each other by four copper wire bands ensured out-of-plane buckling of the assembly during compression testing did not occur. c) Assembly containing single buckled beam spring type occupying all key locations (n_1^v = 0.333 and n_1^o = 0.667). d) Assembly containing single 5-magnet spring type occupying all key locations (n_1^v = 0.333 and n_1^o = 0.667).

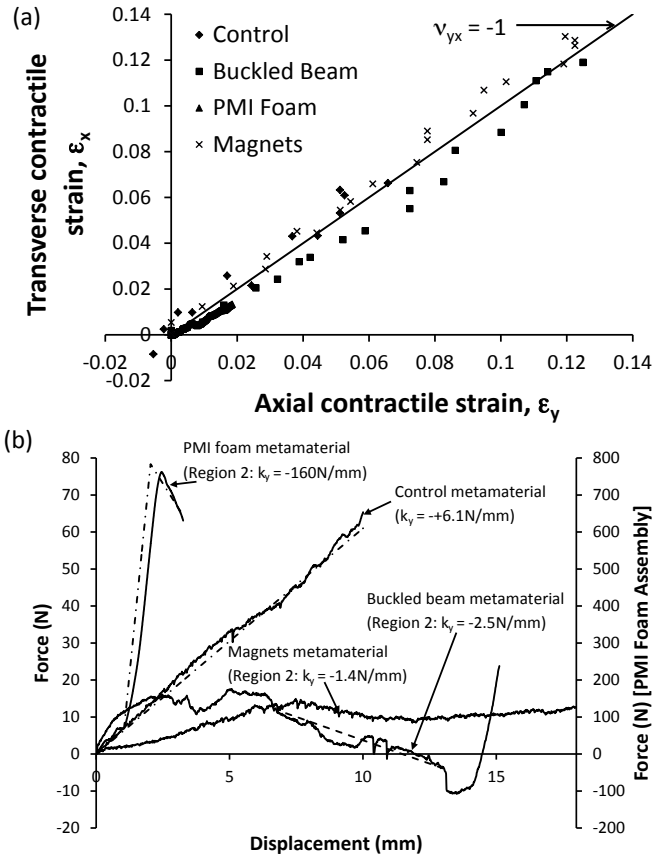

Figure 5. a) Transverse strain as a function of axial strain for assemblies shown in Figure 4a-d. b) Compressive force as a function of compressive axial displacement for assemblies shown in Figure 4a-d. Dot-dashed lines correspond to model predictions based on the measured single-element stiffnesses (Figure 3a and 3b) for the control and PMI foam assemblies (Supporting Information), and the dashed line is the least squares best fit line to the negative stiffness region of the magnets assembly.

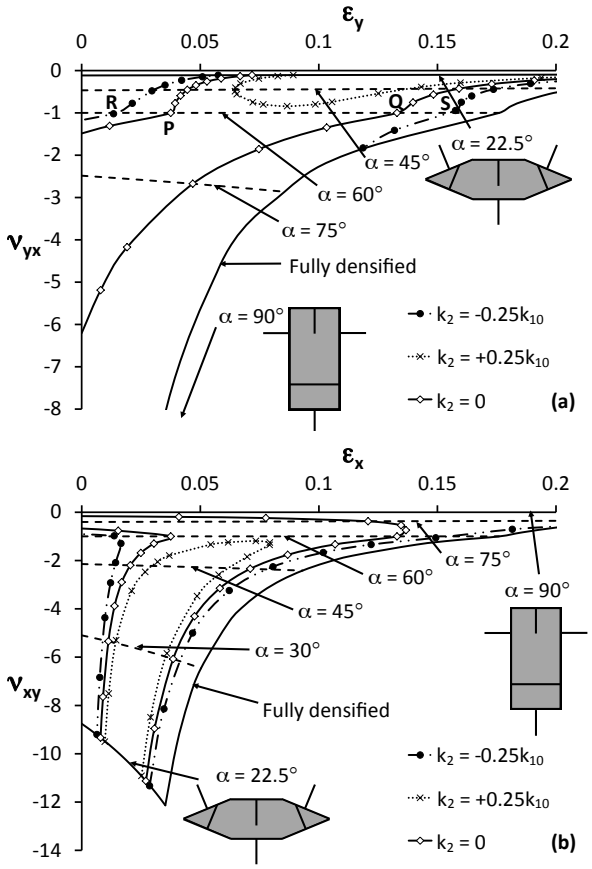

Figure 6. Dependency of mechanical metamaterial properties and strain on sub-unit angle. (a) Incremental Poisson's ratio (ν_{yx}) as a function of global applied compressive strain (ε_y) for an assembly of sub-units of edge lengths $l_1 = l_2$, infinitesimally narrow keyways having depths $\Delta_1 = \Delta_2 = 0.5l_1$, containing a buckled beam spring type (k_1 as in Figure 2a and 2c) occupying all vertical key locations ($n_1^v = 0.333$ and $n_1^o = 0$) and a constant stiffness spring type (k_2) occupying all oblique key locations ($n_2^v = 0$ and $n_2^o = 0.667$). Dashed curves are ν_{yx} vs ε_y data for the cases of $\alpha = 22.5$, 45, 60, 75 and 90° ($\varepsilon_y = 0$ corresponds to the fully expanded structure in each case). Curves with symbols correspond to ν_{yx} vs ε_y data when $E_y = 0$ (for $22.5 < \alpha < 90°$) for $k_2 = -0.25k_{10}$, 0 and $0.25k_{10}$, and define enclosed regions of simultaneous negative Poisson's ratio and negative stiffness response. Points P and Q correspond to the strains where $k_y = 0$ when $k_2 = 0$, and points R and S to the strains where $k_y = 0$ when $k_2 = -0.25k_{10}$, and are the same data points as in Figure 2d for comparison. The boundaries (solid curves) are defined by the fully expanded (zero strain) and fully densified structures, and when one female keyway intersects with another sub-unit edge in the same sub-unit (i.e. when $\alpha = 22.5°$ for the parameter set used here). (b) ν_{xy} vs ε_x for same system as in (a) - curves with symbols correspond to $E_x = 0$.

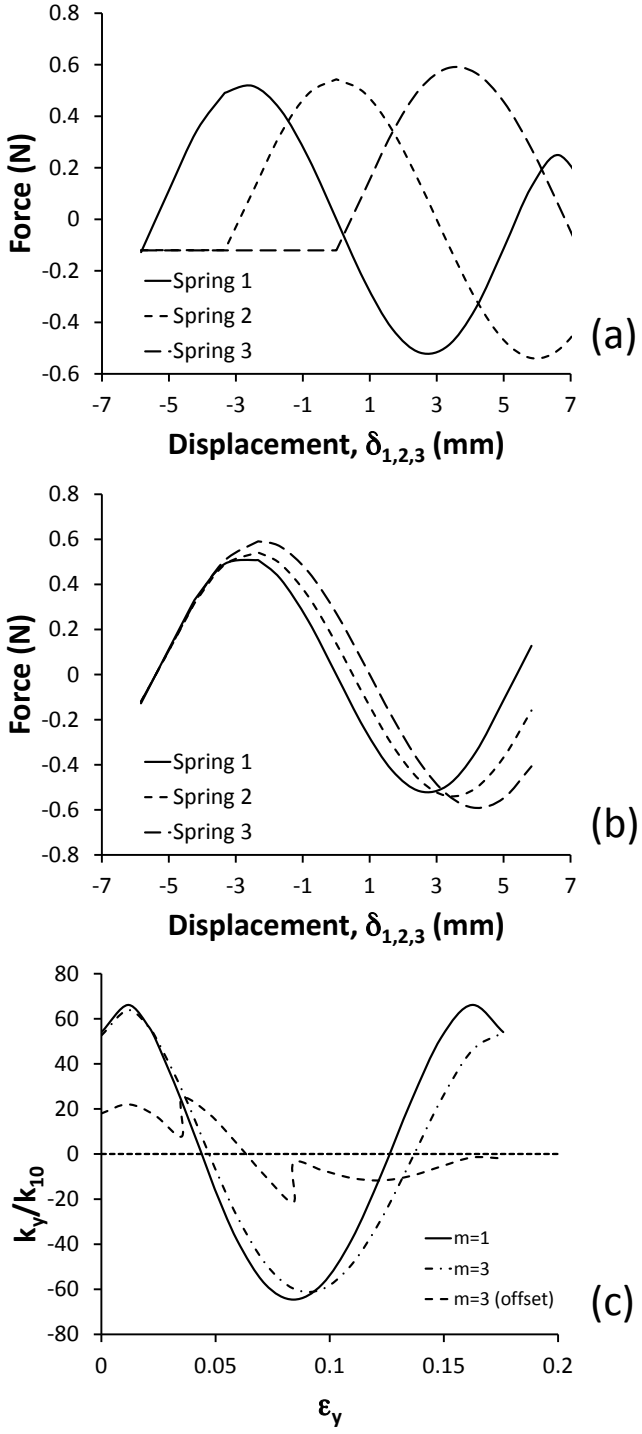

Figure 7. Predicted metamaterial stiffness responses for off-set and/or variable spring configurations in an assembly of keyed regular hexagons. $l_1 = l_2 = 35$ mm, $\alpha = 60°$, $\Delta_1 = \Delta_2 = 0.5l_1$, $a_0 = 0.288l_1$, $\delta_{10} = \delta_{20} = \delta_0 = -0.167l_1$. a) Force-displacement curve for 3 off-set buckled beams (Spring 1: $F = -0.00017707\delta^5 + 0.00000071946\delta^4 + 0.015372\delta^3 - 0.000032436\delta^2 - 0.29619\delta + 0.00021464$; Spring 2: $F = -0.119768451$ when $\delta < -3.33$ mm and $F = -0.00012239\delta^5 + 0.00181690\delta^4 + 0.00157633\delta^3 - 0.07875594\delta^2 + 0.00131133\delta + 0.54337551$ when $\delta > -3.33$ mm; Spring 3: $F = -0.120584879$ when $\delta < 0$ mm and $F = -0.00008587\delta^5 + 0.00294254\delta^4 - 0.02982722\delta^3 + 0.06097563\delta^2 + 0.24200148\delta - 0.12058488$ when $\delta > 0$ mm). b) Force-displacement curve for 3 buckled beams (Spring 1: as in (a); Spring 2: $F = -0.00012239\delta^5 + 0.00028703\delta^4 + 0.012096\delta^3 - 0.017923\delta^2 - 0.27326\delta + 0.13808$; Spring 3: F

= -0.0000858656^5 + 0.00043814δ^4 + 0.00961$4\delta^3$ - 0.03067$1\delta^2$ - 0.25227δ + 0.27256). c) Normalised metamaterial stiffness (k_y/k_{10}) as a function of ε_y for a 3 x 3 array of unit cells with spring type 1 occupying all keyways (m = 1, N = 54, n_1^v = 0.333, n_1^o = 0.667, solid curve), equal numbers of off-set springs 1, 2 and 3 from (a) distributed evenly throughout the system (m = 3, N = 54, $n_1^v = n_2^v = n_3^v$ = 0.111, $n_1^o = n_2^o = n_3^o$ = 0.222, dashed curve), and equal numbers of springs 1, 2 and 3 from (b) distributed evenly throughout the system (m = 3, N = 54, $n_1^v = n_2^v = n_3^v$ = 0.111, $n_1^o = n_2^o = n_3^o$ = 0.222, dot-dashed curve).

The table of contents entry

A scalable mechanical metamaterial simultaneously displaying negative stiffness and negative Poisson's ratio responses is presented. Interlocking hexagonal sub-unit assemblies containing 3 alternative embedded negative stiffness (NS) element types display Poisson's ratio values of -1 and NS values over two orders of magnitude (-1.4 N mm^{-1} to -160 N mm^{-1}), in good agreement with model predictions.

Keywords: mechanical metamaterial, negative stiffness, negative Poisson's ratio, auxetic, mechanical properties

Trishan A. M. Hewage, Kim L. Alderson, Andrew Alderson*, and Fabrizio Scarpa

Double-Negative Mechanical Metamaterials Displaying Simultaneous Negative Stiffness and Negative Poisson's Ratio Properties